International Journal of Engineering Research
Volume No.4, Issue No.8, pp : 412-418
ISSN:2319-6890 (online),2347-5013 (print)
01 August 2015

Steady State Analysis of Wind Driven SM-BDFIG in the Super-Synchronous Range of Operation

Mahmoud A. Saleh, Maged N. F. Nashed, Mona N. Eskander
Electronics Research Institute, Cairo, Egypt
mahmoudsaleh36@yahoo.com , maged@eri.sci.eg , eskander@eri.sci.eg

Abstract: In this paper a simplified mathematical model of a single machine brushless double fed induction generator (SM-BDFIG) connected to a variable speed wind turbine is presented. The SM-BDFIG consists of a slip ring induction machine, which is the main generator, a converter, and a battery pack mounted on the same shaft. In the super-synchronous speed range of operation, which is investigated in this research paper, the rotor voltage is rectified and used to charge the batteries. The steady state performance of the proposed generator is studied at different values of battery open circuit voltage, different values of the battery internal resistance, and different ratios of rotor leakage reactance to rotor resistance. Results revealed that the parameter that had a significant effect on the machine performance is the ratio of rotor leakage reactance to rotor resistance.

Keywords: Single Machine Brushless Doubly-Fed Induction Generator "SM-BDFIG", 3-phase bridge converter, super-synchronous operation, Battery charge, and DC link.

I. Introduction

According to the global wind energy council "GWEC" report [i], the growth in the installed capacity of wind energy conversion systems (WECS) in the year 2014 surpassed the most optimistic predictions. The global total installed capacity increased from 319 GW to nearly 370 GW, i.e. an increase of 51 GW, setting a new record within one year. The forecast for the next five years, 2015-2019, is a growth in WECS installed up to 670 GW, which is expected to add nearly 100,000-150,000 wind generators. . WECS are clean energy sources, affordable, indigenous, reliable, and quick to install.
Nowadays, the DFIG is the common electric generator in newly erected WECS due to its merits of variable speed operation, power control capability, and the lower cost of rotor circuit converter. However, the presence of carbon brushes and slip rings between the rotor circuit and the stationary converter necessitates frequent maintenance. Frequent maintenance can be eliminated by using brushless doubly-fed induction generators (BDFIG). Different designs were proposed for BDFIG [ii-x].
The main concern of this paper is the performance of the single machine BDFIG proposed in [xi], in which the main generator, the converter, and the battery pack are mounted on the same shaft. The main advantages of the SM-BDFIG are the use of a single machine for mechanical to electrical energy conversion, the ability to generate power within wide range of wind turbine speed, and the possibility to be connected to the grid as well as to operate in stand-alone WECS.
Since the SM-BDFIG performance at sub-synchronous and synchronous speeds are similar to the DFIG performance, previously analyzed in detail [xi], thus this paper concentrates on the super-synchronous range of operation of the SM-BDFIG

II. SM-DFIG Configuration

The SM-BDFIG configuration is shown in Fig (1). It consists of a slip ring induction generator with its rotor circuit connected to a six-IGBT converter. The IGBT converter is connected to a battery bank and can be operated in 3 different modes depending on the value of the rotor angular speed ω. If $\omega < \omega_s$ (where ω_s is the synchronous angular speed), it is operated as an inverter fed by the battery bank and feeding the rotor circuit with ac voltage at rotor frequency. At the synchronous speed i.e $\omega=\omega_s$ the second and third rotor phases are connected to one terminal, and dc voltage from the battery is applied between this terminal and the terminal of the first phase, hence the machine is operated as a synchronous generator. If $\omega>\omega_s$, the circuit is operated as a Three Phase Bridge rectifier, changing the rotor circuit voltage into dc used to charge the battery bank. Table I describes the modes of operation of the described circuit.

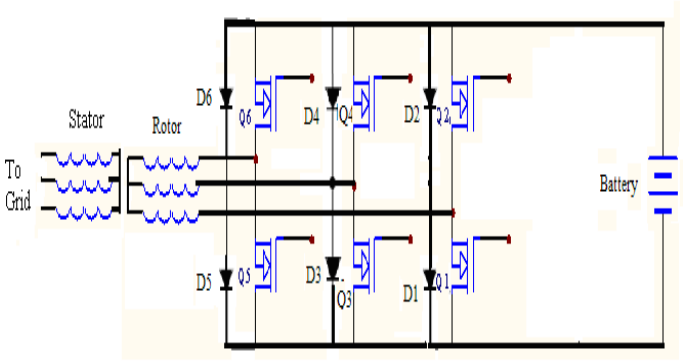

Figure (1) Layout of SM-BDFIG

Table 1: converter operation

Speed	Power Flow	Control
$\omega<\omega_s$	From Battery to rotor	Inverter
$\omega=\omega_s$	DC power from to rotor	Close Q_1 , Q_4 , Q_6
$\omega>\omega_s$	From rotor to battery	Rectifier

To operate the above-described circuit in the correct mode, a controller is designed to read the value of the rotational speed, choose the operation mode, and apply output signals to the

ISSN:2319-6890 (online),2347-5013 (print)
01 August 2015

IGBTs switches according to the required mode of operation. A flow-chart of the proposed controller is given in Fig. (2).

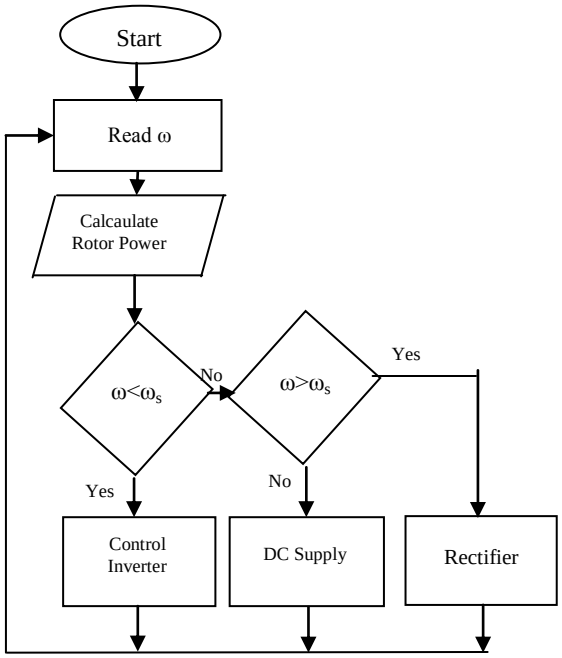

Figure (2) Flowchart of controller.

III. Mathematical Analysis of Steady State Operation of SM-BDFIG

Wind usually blows with speeds starting from zero (calm wind) up to a maximum speed (gust wind). As far as wind energy conversion systems (WECS) are concerned, there are three critical values of wind speed; namely, the cut-in (V_c), rated (V_r), and cut-out speed (V_o) and their corresponding angular speeds of the wind turbine. In most WECS, wind turbine angular speed is kept constant at the rated speed to avoid severe mechanical stresses on the turbine blades. Hence, the wind turbine operates between the cut-in and cut-out speed and is stopped (either by braking or by blade pitch control) outside this range. The wind turbine angular speed ranges between the speed corresponding to the wind cut-in speed ω_c and the speed corresponding to the rated wind speed ω_r.

The DFIG coupled to the wind turbine via a gear box operates in the range between ω_c and ω_r. However, in the case of the DFIG, there exists a critical angular speed ω_s, which is the synchronous speed. Hence three ranges of operation exist, the sub-synchronous range ($\omega_c \le \omega < \omega_s$), the synchronous speed ($\omega= \omega_s$,) and the super-synchronous range ($\omega_r \ge \omega > \omega_s$).

In the super-synchronous range of operation, the wind turbine mechanical power P_m is applied to the SM-BDFIG to be converted to electrical power. At steady state, the mechanical torque T_m exerted by the wind turbine, is balanced by the electromagnetic torque T_e produced by the interaction of the magnetic fields in the air gap of the SM-BDFIG,

$$\text{i.e. } T_m = \frac{P_m}{\omega} = T_e = \frac{P_g}{\omega_s} \qquad (1)$$

Where: P_g is the air gap power transferred from the SM-BDFIG rotor to its stator via the air gap. Manipulating equation (1) gives:

$$P_m = \frac{\omega}{\omega_s} P_g = (1+s)P_g \qquad (2)$$

Hence, part of the wind turbine mechanical power is converted to electrical power P_g, and transferred via the air gap to the stator, then to the grid or electrical load, after deducting the stator copper and iron losses. The remainder of the mechanical power sP_g is converted to dc power via the three-phase bridge rectifier, after deducting the rotor copper losses and the rectifier losses. If the terminal voltage of rotor phase "1" is: $V_m \cos \alpha$, then the dc bridge voltage V_b , shown in Fig 3, applied across the battery terminals, is expressed as [xii]:

$$V_b = \frac{3\sqrt{3}}{\pi} V_m [1 - \sum_{k=1}^{\infty} \frac{2}{36k^2 - 1} \cos(6k\alpha)] \qquad (3)$$

Where, V_m= maximum value of rotor phase voltage
α = s.p. ω.t
s.p. ω = angular frequency of the rotor at any slip s
s = slip
p = number of pole pairs of the DFIG
t=time

At any state of charge SOC, the battery can be represented by a constant voltage V_{oc} and an internal resistance R_b

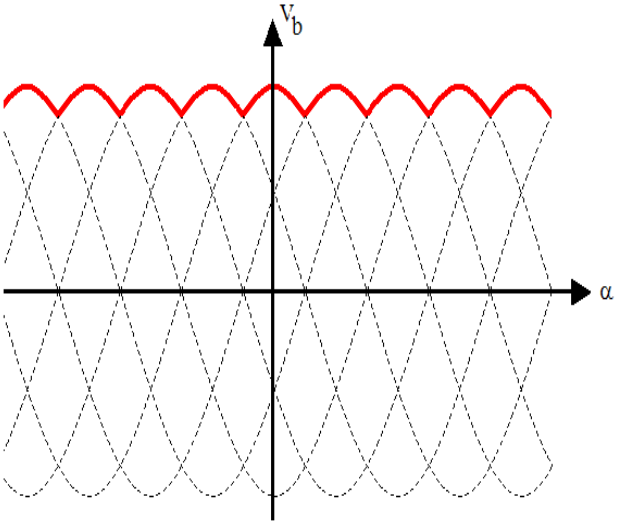

Figure (3) Wave form of voltage across the battery terminal.

$$V_b = V_{oc} + I_b R_b = \frac{3\sqrt{3}}{\pi} V_m [1 - \sum_{k=1}^{\infty} \frac{2}{36k^2 - 1} \cos(6k\alpha)] \qquad (4)$$

$$V_b = \frac{3\sqrt{3}}{\pi} V_m [1 - \frac{2}{35}\cos 6\alpha - \frac{2}{143}\cos 12\alpha .....] \qquad (5)$$

It is clear from equation (5) that the harmonic components in battery voltage are marginal and could be neglected. Therefore:

$$V_b \cong \frac{3\sqrt{3}}{\pi} V_m$$

Consequently, the battery current will be considered as DC current with constant amplitude i.e.

ISSN:2319-6890 (online),2347-5013 (print)
01 August 2015

$$I_b = \frac{V_b - V_{oc}}{R_b} \cong \frac{1}{R_b}[\frac{3\sqrt{3}}{\pi} V_m - V_{oc}] \qquad (6)$$

The wave forms of the currents i_1, i_2, i_3 in the rotor phases are shown in Fig 4.

The Fourier expansion of current i_1 in phase 1 of the rotor circuit can be expressed as:

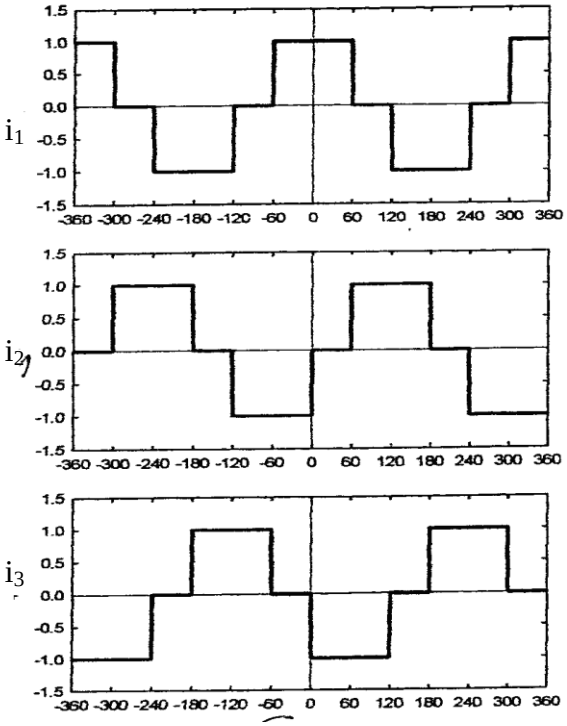

Figure (4) Wave forms of the currents in different phases.

$$i_1 = \frac{2\sqrt{3}}{\pi} I_b[\cos\alpha - \frac{1}{5}\cos 5\alpha + \frac{1}{7}\cos 7\alpha - \frac{1}{11}\cos 11\alpha.....] \qquad (7)$$

From equations (6) and (7), the current in phase 1 of the DFIG can be expressed as:

$$i_1 = \frac{1}{R_b}(\frac{3\sqrt{3}}{\pi} V_m - V_{oc})[\cos\alpha - \frac{1}{5}\cos 5\alpha + \frac{1}{7}\cos 7\alpha - \frac{1}{11}\cos 11\alpha.....] \qquad (8)$$

The fundamental component of the current i_1 is i_{1f} , where

$$i_{1f} = \frac{2\sqrt{3}}{\pi}\frac{1}{R_b}(\frac{3\sqrt{3}}{\pi} V_m - V_{oc})\cos\alpha \qquad (9)$$

As previously mentioned,

$$v_1 = V_m \cos\alpha$$

Assuming that the induced voltage in the rotor phase 1 leads the current in phase 1 by an angle ϕ electrical degree, hence the instantaneous value of the rotor induced voltage at any slip may be expressed as:

$$e_1 = sE_m \cos(\alpha + \phi)$$

Where E_m is the maximum value of the rotor induced voltage per phase at standstill.

Under steady state operating conditions of the SM-BDFIG, the RMS values of the currents ($\dot{I}_{1f}$) and voltages ($\dot{V}_1, \dot{E}_1$) can be expressed in complex form as:

$$\dot{V}_1 = \frac{V_m}{\sqrt{2}}, \qquad \dot{I}_{1f} = \frac{\sqrt{6}}{\pi}\frac{1}{R_b}(\frac{3\sqrt{3}}{\pi} V_m - V_{oc}) \qquad (10)$$

$$\dot{E}_1 = \frac{sE_m}{\sqrt{2}}[\cos\phi + j\sin\phi)$$

The currents and voltages in phase 1 are related at any slip as:

$$\dot{E}_1 = \dot{V}_1 + \dot{I}_{1f}(R_r + jsX_r) \qquad (11)$$

R_r and X_r are rotor resistance and leakage reactance per phase.

From equations (10) and (11) we can write:

$$s\frac{E_m}{\sqrt{2}}\cos\phi = \frac{V_m}{\sqrt{2}} + \frac{\sqrt{6}}{\pi}\frac{R_r}{R_b}(\frac{3\sqrt{3}}{\pi} V_m - V_{oc}) \qquad (12)$$

$$s\frac{E_m}{\sqrt{2}}\sin\phi = s\frac{\sqrt{6}}{\pi}\frac{X_r}{R_b}(\frac{3\sqrt{3}}{\pi} V_m - V_{oc})$$

Equation (12) can be rewritten after some mathematical manipulations as follows:

$$V_m^2[1 + 3.21(1 + s^2\beta^2)(\frac{R_r}{R_b})^2] - V_m V_{oc}[3.97(1 + s^2\beta^2)(\frac{R_r}{R_b})^2 + +2.21\frac{R_r}{R_b}] + 1.20(1 + s^2\beta^2)(\frac{R_r}{R_b})^2 V_{oc}^2 - s^2 E_m^2 = 0 \qquad (13)$$

$$E_m \sin\phi = 1.10\frac{X_r}{R_b}(1.65V_m - V_{oc}) \qquad (14)$$

Where $\beta = \frac{X_r}{R_r}$

The maximum value of the fundamental component of the rotor current in phase one is

$$I_{1f} = \frac{1.82}{R_b}(V_m - 0.61V_{oc}) \qquad (15)$$

$$P_g = \frac{3}{2} s I_{1f} E_m \cos\phi \qquad (16)$$

IV. Numerical results

Using equations 13-16, a number of performance indicators for a 1.50 MVA SM-BDFIG (Appendix) is calculated and the numerical results are demonstrated in the group of figures 5, 6 and 7. Different values for the battery pack state of charge (SOC) are assumed, to evaluate the effect of the battery internal resistance and open circuit voltage on the performance of the SM-BDFIG. The variation of the rotor terminal voltage V_m with the rotor relative angular speed $\gamma = \omega/\omega_s$ (and the slip s) for different values of battery open circuit voltage V_{oc} is shown in Fig. 5a. It is shown that a 23% change in the value of V_m corresponds to tripling the magnitude of V_{oc}.

The variation of the rotor terminal voltage V_m with the rotor relative angular speed $\gamma = \omega/\omega_s$ (and the slip s) for different values of battery internal resistance R_b is shown in Fig.6a. The rotor voltage increased to 2.70 of its value corresponding to tripling the value of R_b. This large variation in V_m is due to the change in the ratio of the rotor leakage inductance to the rotor

ISSN:2319-6890 (online),2347-5013 (print)
01 August 2015

resistance (β) as R_b increases. The significant effect of β on the machine performance is verified in Figs. 7a till 7d.

The variation of the rotor terminal voltage V_m with the rotor relative angular speed $\gamma = \omega / \omega_S$ (and the slip s) for different ratios of rotor leakage reactance to rotor resistance β of the DFIG is shown in Fig 7a. A 1.87 increase in Vm corresponded to a 2.50 variation in the value of β, revealing the significant effect of β on V_m.

Figures 5b, 6b, and 7b show the variation of the rotor power factor with γ (and s), for different values of V_{oc}, R_b, and β respectively. The marginal effect of V_{oc} on the power factor is evident. However, the power factor increased to 5 times its value as R_b increased to three times its value. Similarly, large variation in p.f. is due to the change in the ratio of the rotor leakage inductance to the rotor resistance (β) as R_b increases. This is evident from Fig.7b, where a significant change in PF occurred as β varies from a ratio of 10 to 25.

Figures 5c, 6c, and 7c show the variation of the fundamental component of the rotor current (I_f) with γ (and s), for different values of V_{oc}, R_b, and β respectively. The marginal effect of V_{oc} on the fundamental component of the rotor current is clear. However, I_f increased to 1.15 of its value as R_b decreased to 0.33 of its value. A significant increase in I_f (to 1.5 times its magnitude) occurred as β varies from a ratio of 10 to 25.

Figures 5d, 6d, and 7d show the variation of the air gap power (approximately the output power of the machine) with γ (and s), for different values of V_{oc}, R_b, and β respectively. The marginal effect of V_{oc} the air gap power is clear. However, P_g varied significantly as R_b decreased to 0.33 of its value. It is emphasized that this large variation is due to the inherent variation in β. This is evident in Fig. (7d), since Pg varied significantly as β varies from a ratio of 10 to 25.

a. At different values of V_{oc}

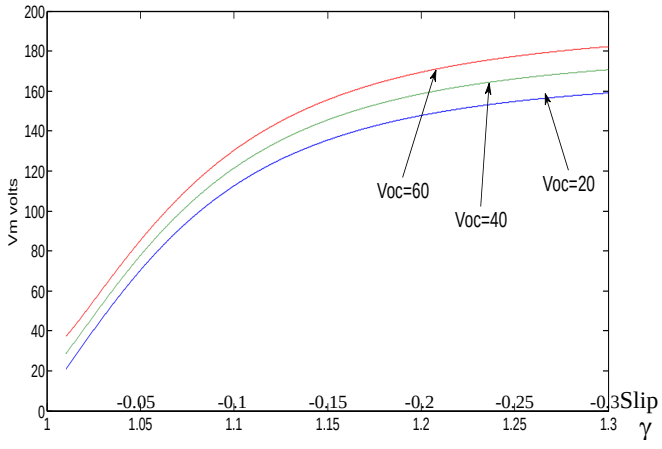

Figure (5a) Rotor Terminal Voltage for Different Values of Battery Open Circuit Voltage.

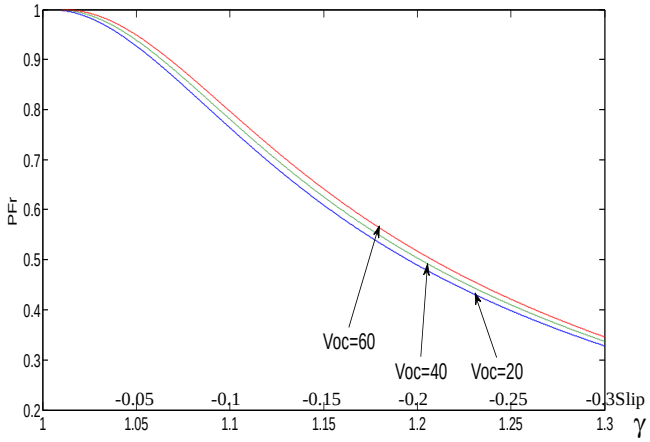

Figure (5b) Rotor Power Factor for Different Values of Battery Open Circuit Voltage.

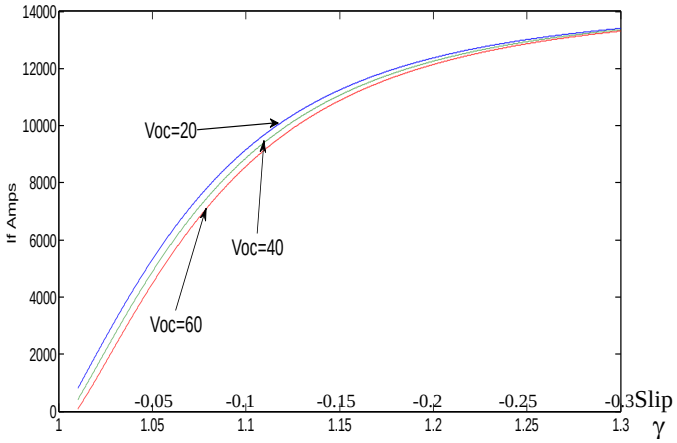

Figure (5c) Fundamental Component of Rotor Current for Different Values of Battery Open Circuit Voltage.

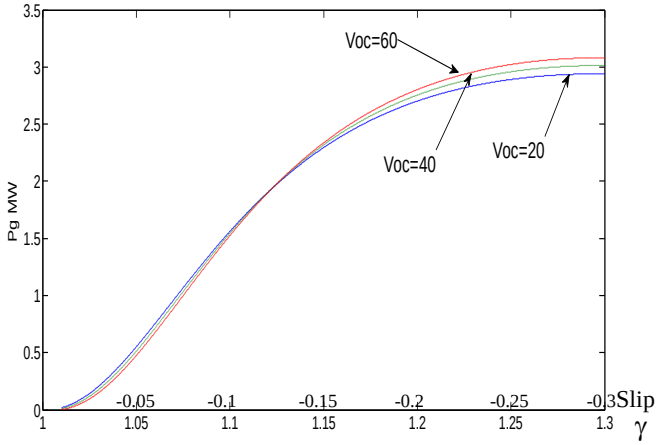

Figure (5d) Air gap Power for Different Values of Battery Open Circuit Voltage.

ISSN:2319-6890 (online),2347-5013 (print)
01 August 2015

b. At different values of battery Resistance

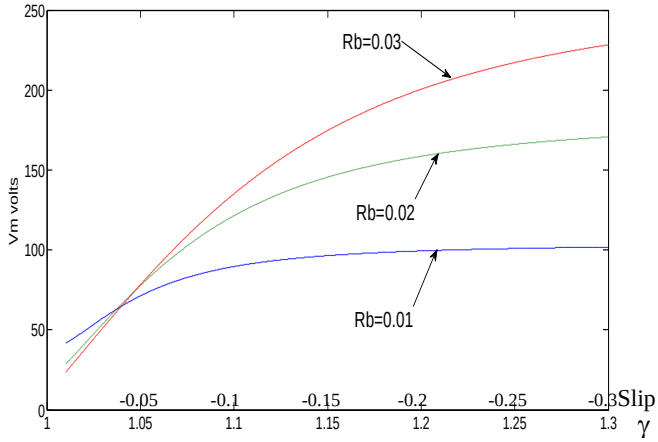

Figure (6a) Rotor Terminal Voltage for Different Values of the Battery internal Resistance.

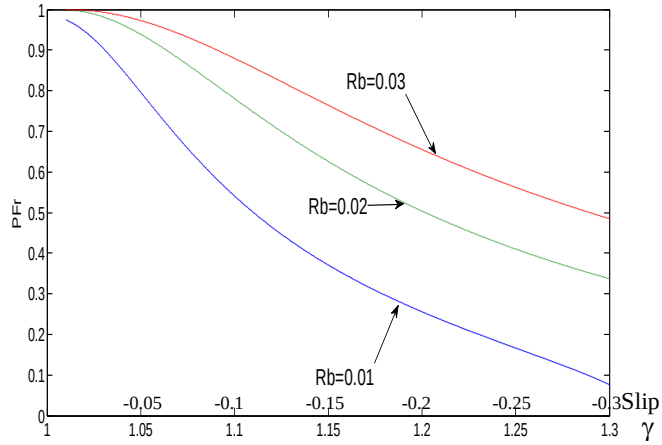

Figure (6b) Rotor Power Factor for Different Values of the Battery internal Resistance.

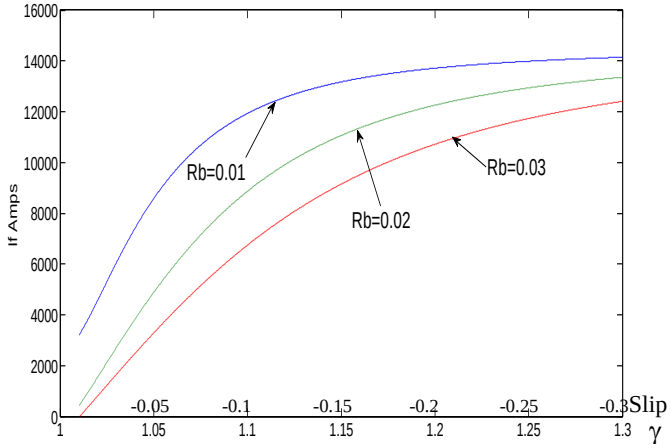

Figure (6c) Fundamental Component of Rotor Current for Different Values of the Battery internal Resistance.

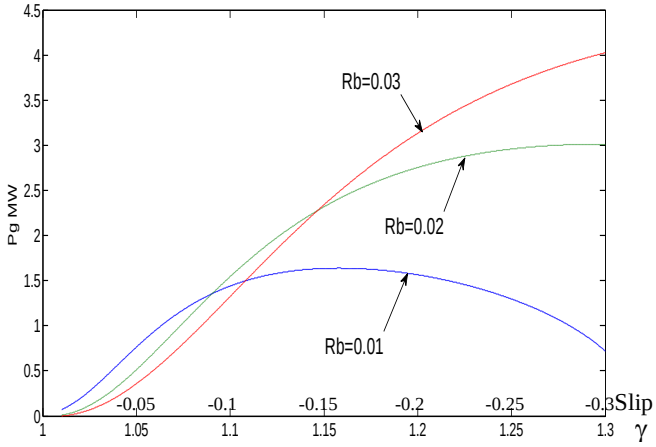

Figure (6d) Air Gap Power for Different Values of the Battery internal Resistance.

c. At difference values of β

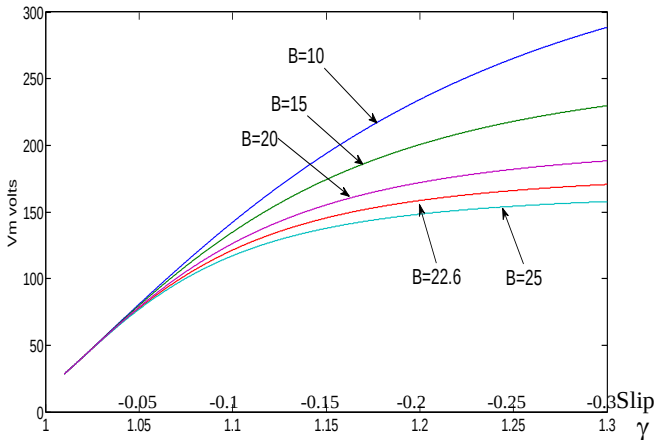

Figure (7a) Rotor Terminal Voltage for Different Values of β.

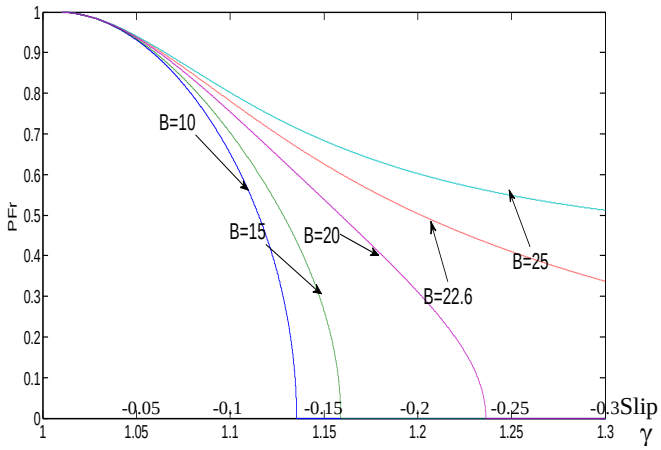

Figure (7b) Rotor Power Factor. for Different Values of β.

ISSN:2319-6890 (online),2347-5013 (print)
01 August 2015

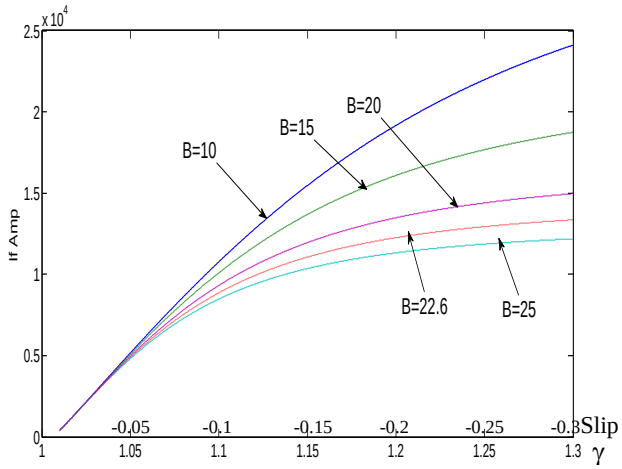

Figure (7c) Fundamental Component of Rotor Current for Different Values of β.

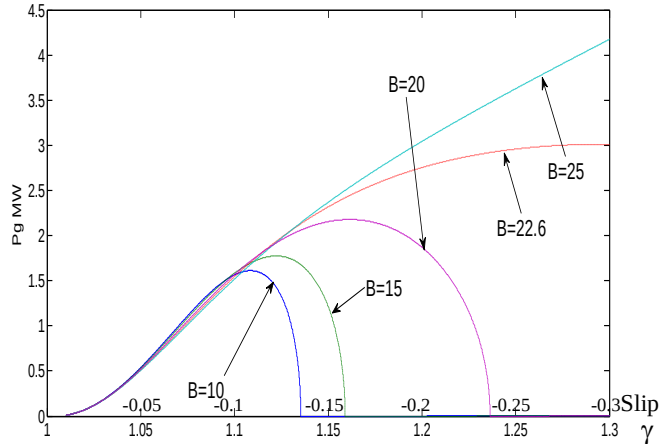

Figure (7d) Air gap Power for Different Values of β.

It is concluded from the above shown set of curves that the change in the open circuit voltage of the battery has a marginal effect on the performance of the SM-BDFIG. However, the battery resistance R_b affected the performance of the generator due to its inherent inclusion in the ratio of rotor leakage reactance to the rotor resistance β. The effective parameter on the performance of the SM-BDFIG, and also all types of DFIGs, is shown to be the ratio of the rotor leakage reactance to the rotor resistance β. This should be seriously taken into consideration during the design process of the induction machine.

V. Conclusion

The simplified mathematical model of the specially designed SM-BDFIG connected to a variable speed wind turbine is presented. The model is simulated by Matlab/simulink to investigate the steady state performance of the proposed generator. The performance of the rotor voltage, the power factor, the fundamental magnitude of the rotor current, and the air gap power at steady state are investigated for the super synchronous speed range, for different values of the battery pack state of charge (SOC). The SOC affects the magnitude of the battery open circuit voltage and the battery internal resistance. The machine performance is also examined at different values of the ratio between rotor leakage reactance to rotor resistance (β).

Results revealed that the change of the batteries' open circuit voltage during the charging period (the super synchronous range of operation) of the battery pack has marginal effect on the performance of the SM-BDFIG. However, the significant changes in the SM-BDFIG performance was due to the variation in β. It is concluded that the induction machines with higher ratio of rotor leakage reactance to rotor resistance are more adequate for operation as SM-BDFIG.

The mathematical analysis, the numerical results and the proposed scheme of operation of the electronic converter presented in this paper could be of great help to the designers as well as the manufacturers of the SM-BDFIG.

Appendix

a- Induction generator ratings

Rated MVA	1.5 MVA
Rated Voltage	0.69 kV line-to-line
Number of poles	6
Rated frequency	60 Hz
Stator/rotor turns ratio	0.379

b- Induction generator parameters

Stator winding resistance	0.005	pu
Rotor winding resistance	0.0021	pu
Stator leakage reactance	0.08	pu
Rotor leakage reactance	0.0478	pu
Magnetizing reactance	6.8	pu
Angular moment of inertia	0.578	sec

References

i. "*Global Wind Report 2014" published by Global wind energy council http://www.gwec.net/publications/global-wind-report-2/global-wind-report-2014-annual-market-update/ February 2015*

ii. Hopfenspergor B, Atkinson DJ, and Lakin RA, "Stator flux oriented control of a cascaded doubly-fed machine" IEE Electric Power Applications, Vol. 46, No. 6, 1999; pp: 597-605.

iii. Protesenke K, and Xu D, "Modeling and control of BDFIG in wind energy applications" IEEE Trans. Power Electronics, Vol. 23, No. 3, 2008, pp:1191-1197.

iv. Cardenas R, Pena R, and Clare J. "Control of a wind generation system based on brushless doubly-fed induction generator fed by a matrix converter" Electric Power Systems Research. Vol. 103, 2013, pp: 49-60.

v. Zhou D, Spec R, and Alexander GC. "Experimental evaluation of a rotor flux-oriented control algorithm for brushless doubly fed machine" IEEE Trans. Power Electronics, Vol. 12, 1997, pp: 72-78.

vi. Duro Basic, Jian Guo Zhu, and Gerard Boardmau, "Transient performance study of a brushless doubly fed twin stator induction generator" IEEE Trans. Energy Conversion, Vol. 18, No. 3, 2003; pp: 400-408.

ISSN:2319-6890 (online),2347-5013 (print)
01 August 2015

vii. Bimal K. Bose, "Modern Power Electronics and Electrical Drives", Prentice-Hall, Inc., ISBN:0-13-016743-6, 2002.

viii. Ruviaro M, Runcos F, Sadowski N, and Borges "IM. Design and analysis of a brushless doubly induction machine with rotary transformer" International Conference of Electrical Machine, ICEM, Rome, Italy, 2010.

ix. Ruviaro M, and Runcos F. "A brushless doubly induction machine with flat plane rotary transformer" International Conference of Electrical Machine, ICEM, Marseille, France, 2012.

x. Rahman Malik N, and Sadarangani C. "Brushless doubly induction machine with rotating power electronic converter for wind power applications", International Conference of Electrical Machine, ICEM, Beijing, China, 2011.

xi Mahmoud A. Saleh and Mona N. Eskander, "A Single Machine Brushless DFIG for Grid-Connected and Stand-Alone WECS", British Journal of Applied Science & Technology, Vol. 4, No. 24, 2014 pp: 3550-3562.

xii. Bimal K Bose ,"Modern Power Electronics and AC Drives" Textbook published by 2002 Prentice-Hall,Inc, ISBN;0-13-016743-6